Scientific Research Publishing

Journal of Materials Science and Chemical Engineering, 2022, 10, 27-48
https://www.scirp.org/journal/msce
ISSN Online: 2327-6053
ISSN Print: 2327-6045

UV-LED Curing Cationic Passivation Film for the Surface of Hot-Dip Aluminum-Zinc Coated Steel Plate

Weixing Lu, Linling Wu, Chunyu Ma, Qian-Feng Zhang*

Institute of Molecular Engineering and Applied Chemistry, Anhui University of Technology, Ma'anshan, China
Email: *zhangqf@ahut.edu.cn

How to cite this paper: Lu, W.X., Wu, L.L., Ma, C.Y. and Zhang, Q.-F. (2022) UV-LED Curing Cationic Passivation Film for the Surface of Hot-Dip Aluminum-Zinc Coated Steel Plate. *Journal of Materials Science and Chemical Engineering*, **10**, 27-48.
https://doi.org/10.4236/msce.2022.109003

Received: July 20, 2022
Accepted: September 27, 2022
Published: September 30, 2022

Abstract

The surface treatment technology of hot aluminum-zinc steel plate and UV curing technology may be effectively combined in the present research. According to different light curing mechanisms, different formulations from UV curing surface treatment agents can be applied to the surface treatment of hot aluminum-zinc steel plate, mainly including 3-ethyl-3-benzoxy-methyl oxacyclobutane (TCM 104) and 3,4-epoxy-cyclohexylformic acid -3',4'-epoxy-cyclohexyl methyl ester (UVR 6110) as active diluents, high molecular weight polyfunctional oxacyclobutane as oligomer, triaryl sulfonium salt as a cationic photoinitiator, and an anthracene compound as a sensitizer. 385 nm LED lamp used as a radiation resource, the effects of the proportion of active diluent, the type and amount of photoinitiator, the amount of sensitizer, the curing temperature, and the amount of nano-SiO_2 on the photocuring rate were investigated by photoper-scanning differential calorimetry (Photo-DSC). The experimental results show that the system has the fastest photocuring rate under the conditions of 8:2 ratio of TCM 104 to UVR 6110, 2.5% photoinitiator, 0.6% sensitizer, 0.2% nano-SiO_2 additive, and 80˚C curing temperature. Based on addition of the appropriate number of various additives, the cationic photocuring surface treatment solution was prepared and further coated on the hot-dip galvalume steel plates. After curing, the passivation films were characterized by neutral salt spray test (NSST), Fourier transform infrared spectroscopy (FT-IR), electrochemical testing and other methods. The results show that the formulations could be cured at an energy of 150 mJ/cm^2, and the overall performance of the passivation film could meet with the requirements of the downstream users.

Keywords

Cationic Photocuring, Hot-Dip Galvalume Steel Plate, Surface Treatment, Corrosion Resistance, Chromium Free Environmental Passivation Film

1. Introduction

Cationic photocuring is a process involving in a photoinitiator initiating the polymerization of epoxy group or vinyl ether by Lewis acid or super protonic acid after ultraviolet radiation. The initiator system has the advantages of low shrinkage, high adhesion, and low odor [1]. In the early period of photocuring, high pressure mercury lamps were commonly used as radiation sources, mainly because of its low cost and broad spectral range. However, the highly pollution and low luminous efficiency of the mercury lamps limit its application, and UV-LED will become the mainstream light source of photocurable technology with the continuous improvement of UV-LED light source technology. At present, the maximum absorption wavelength of cationic photoinitiators in the field of ordinary photocuring ranges from 220 nm to 300 nm, which is difficult to compete with the long-wave UV-LED light source. Thus, it is necessary to select an appropriate sensitizer (as shown in **Figure 1**) to improve the maximum absorption wavelength of cationic photoinitiators.

Although oxyheterocyclobutane compounds have the advantages of low viscosity, high adhesion, low shrinkage, low toxicity and non-volatile, the scope of their application has been limited due to their slow photocuring rate. From the mechanism of oxygen heterocyclic butane monomer trigger mechanism, the process of ring opening polymerization formed the three-level oxonium salt (as shown in **Figure 2**), and the salt has high stability, so that this kind of compounds compared with epoxy ethane has more obvious induction period, but this period is slowly, possibly owing to the oxygen heterocyclic butane polymerization rate [2] [3].

Related studies have shown that aliphicyclic epoxides have a promoting effect on the photopolymerization of oxacyclic butane, and such compounds can significantly reduce the induction period of the ring-opening polymerization of oxacyclic butane cationic. This effect of lowering the induction is known as the "kick-starting" effect [4]. Such compounds that reduce the induction are called "kick-starting" reagents [5] [6]. According to this background, a mixture of oxygen heterocyclic butane and epoxy ethane in a certain proportion was selected as the reactive diluent to increasing the light curing rate.

2. Experiments

2.1. Components Selection and Conditions Optimization

The selection of each component in the system is listed in **Table 1**, the selection and optimal proportion of each component were determined by photodifferential scanning calorimetry (photo-DSC), which is the most widely used technology in the study of photocuring reaction [7]. It is quiet suitable for the determination of kinetic parameters, such as enthalpy, conversion rate, rate constant, Arrhenius parameters, etc. The instrument setup is shown in **Figure 3** [8]. The main limitation of photo-DSC is that the reaction time is relatively long and it is not possible to accurately monitor the polymerization reaction occurring within 10 s, thus it needs to be operated under low-intensity ultraviolet radiation [9]-[14].

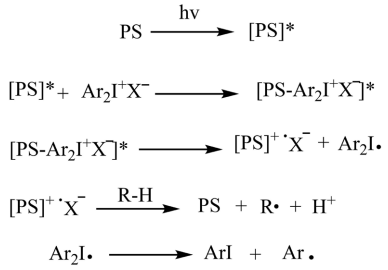

Figure 1. Anthracene sensitizer to sulfonium salt sensitizer mechanism equation.

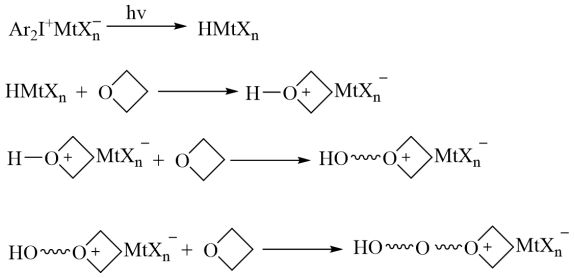

Figure 2. Reaction equations for ring opening polymerization of oxacyclobutane cations [4].

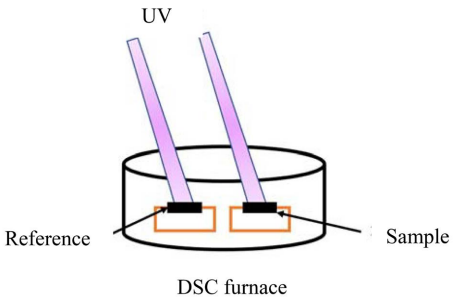

Figure 3. Instrument Settings of Photo-DSC.

Table 1. Basic equations of photocurable passivation solution.

component	mass percent wt%
Active thinner (ternary epoxy + quaternary epoxy)	96% - 99%
Oligomer	0%
Ctionic photoinitiator	1% - 4%
Additives	0%

2.1.1. Selection of Cationic Photoinitiator

Four clean beakers were respectively filled with 9.7 g of the mixture of ternary epoxy and quaternary epoxy at a ratio of 1:1, and then four photoinitiators were added with 0.3 g each to obtain the basic test. The results of the photo-DSC testing showed that the four cationic photoinitiators had high photoinitiation rates. As shown in **Figure 4**, four different cationic photoinitiators (structures shown in **Figure 5**) (Changzhou Qiangli Company, technology grade) were selected to

test their photocuring rate through photo-DSC, and their heat release per unit mass was calculated by integrating the four curves. Photoinitiator-1 is triaryl sulfonium hexafluoroantimonate. Photoinitiator-2 is triaryl sulfonium hexafluorophosphate (single and double salt mixture). Photoinitiator-3 is triaryl sulfonium hexafluorophosphate (single and double salt mixture), and Photoinitiator-4 is diaryliodinium hexafluoroantimonate. It can be seen from **Figure 4** that Photoinitiator-4 has the fastest photoinitiation rate and the lowest heat release per unit. Photoinitiator-4 has high photoinitiation efficiency and the curing degree of its system is low. The photocuring rate of Photoinitiator-3 is slightly lower than that of Photoinitiator-4, and the highest heat release per unit mass indicates that the curing degree of the system is the highest. Because the cost of iodonium salt is much higher than that of sulfonium salt, it is difficult to be used in the field of ordinary photocuring, so Photoinitiator-3 is chosen as the photoinitiator. As displayed in **Figure 6** and **Figure 7**, the ultraviolet absorption spectra of four cationic photoinitiators and one anthracene sensitizer were tested. **Figure 6** shows that the four cationic photoinitiators all had strong absorption at about 260 nm and 300 nm, on which Photoinitiator-3 had the strongest absorption at about 300 nm. Because the light source UV-LED's spectral range arrive at 385 nm, and the four photoinitiators have no absorption at 385 nm, an anthracene sensitizer with strong absorption at 385 nm is selected to sensitize the cationic photoinitiator, so as to indirectly increase the maximum absorption wavelength.

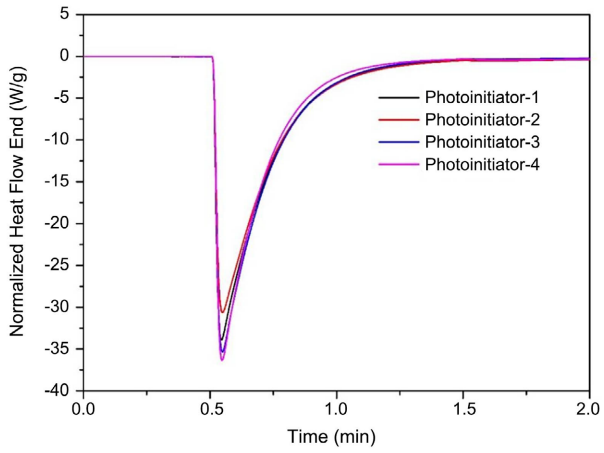

Figure 4. Photoinitiator rate and curing heat release of four different photoinitiators for the comparison.

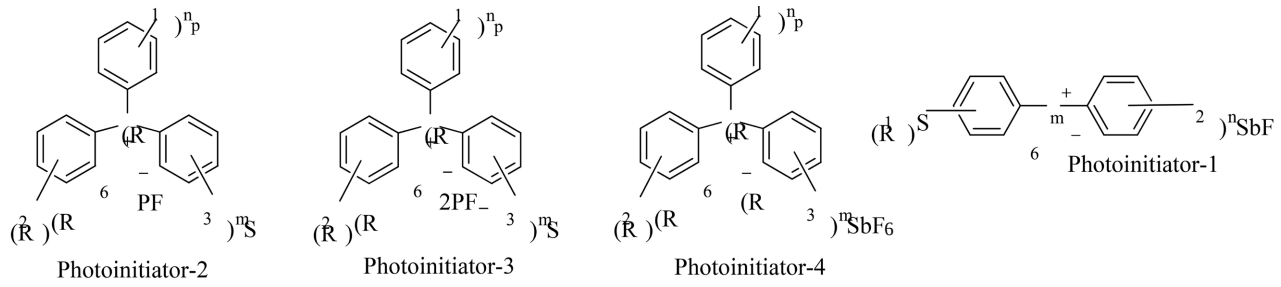

Figure 5. Structures formula of four different photoinitiators (Changzhou Qiangli Company, technology grade).

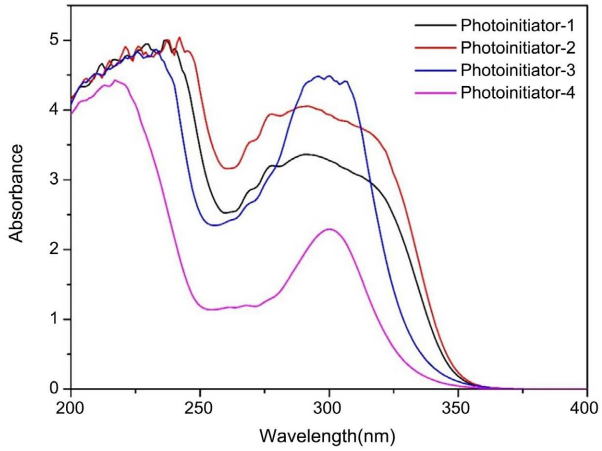

Figure 6. UV absorption profile of four photoinitiators.

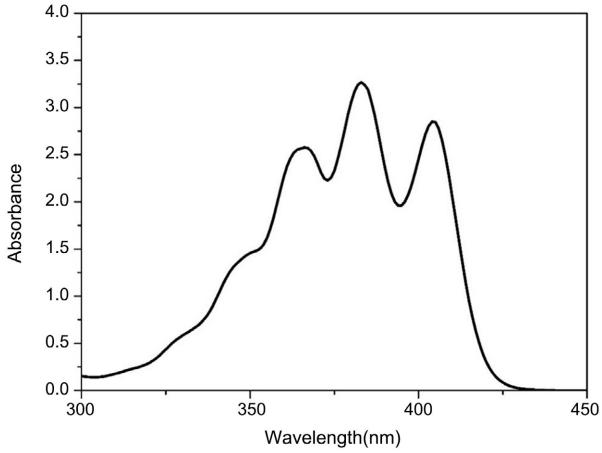

Figure 7. UV absorption spectrum of sensitizer.

2.1.2. Effect of the Amount of Photoinitiator on the Speed of Photocuring

As shown in **Figure 8** and **Figure 9**, the effects of different dosage of photoinitiator on curing rate and curing degree were tested. Photoinitiator-3 triaryliodonium hexafluorophosphate (single salt) was used as cationic photoinitiator with the addition ratio of 1% - 4% and active thinner of 96% - 99%, in which the ratio of ternary ring and quaternary ring was in 1:1. As from **Figure 8**, when the dosage of photoinitiator is 2.5%, the curing rate is the fastest. And when the dosage of photoinitiator is higher than 2.5%, the curing rate decreases, the degree of curing increases slightly either. Therefore, 2.5% dosage was selected as the optimal addition amount.

2.1.3. Effect of Sensitizer Dosage on Photocuring Speed

As shown in **Figure 10** and **Figure 11**, the effects of the dosage of sensitizer on curing rate and degree were tested. 2.5% Photoinitiator-3 triaryliodonium hexafluorophosphate (single salt) was used as cationic photoinitiator, an anthracene compound was used as sensitizer, and the dosage of active thinner was 96.5% - 97.5%. The ratio of ternary and quaternary rings is in 1:1. In **Figure 10**, it has the fastest reaction rate when the sensitizer is 0.6%, when the amount of sensitizer is

greater than 0.6%, the curing rate decreases and the heat release per unit mass increases slightly as well. Considering comprehensively, choose 0.6% as the optimal dosage of sensitizer.

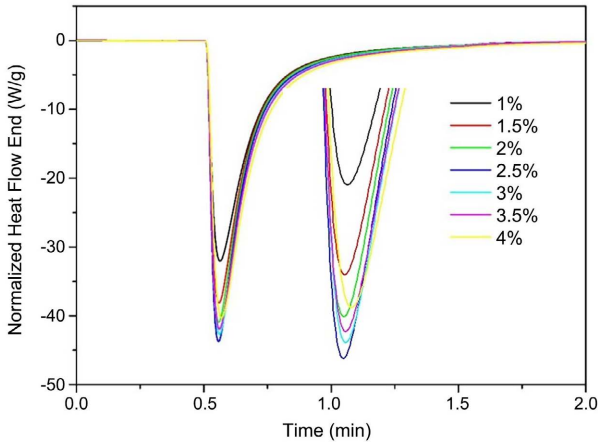

Figure 8. Effect of photoinitiator dosage on curing rate.

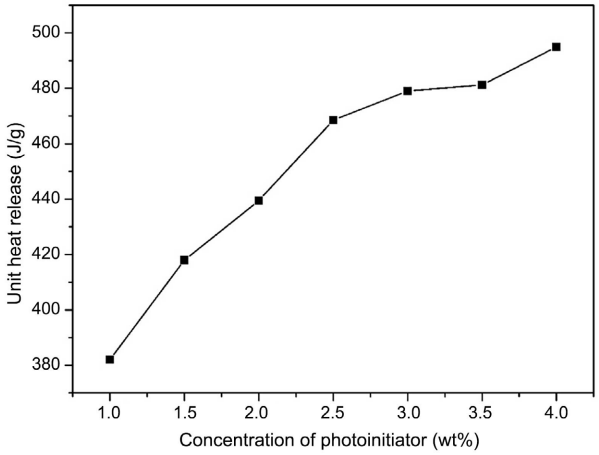

Figure 9. Influence of photoinitiator dosage on curing degree.

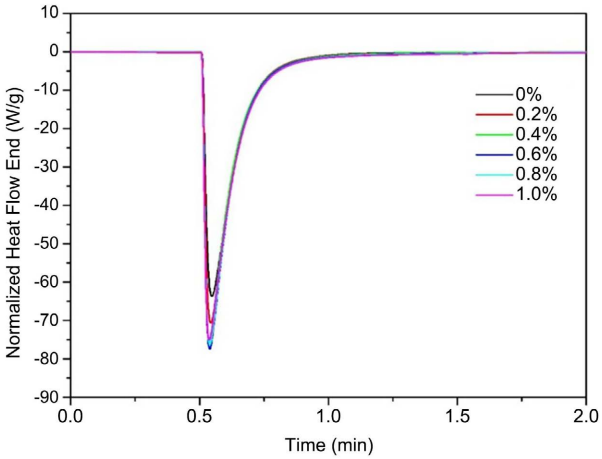

Figure 10. Effect of the dosage of anthracene sensitizer on the photocuring rate.

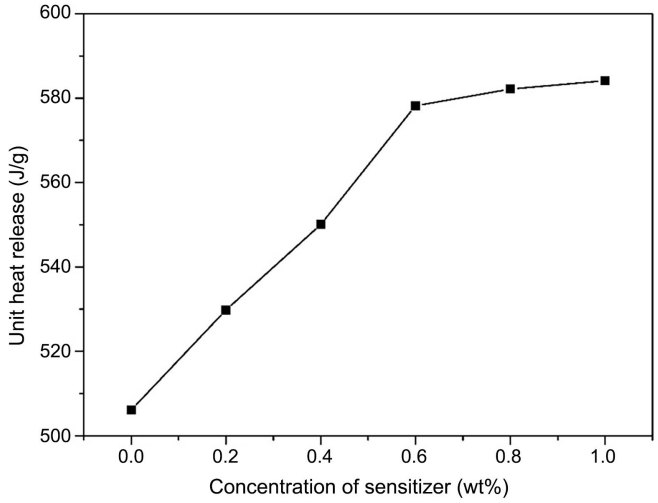

Figure 11. Influence of sensitizer dosage on curing degree.

2.1.4. Selection of Active Diluent (Monomer)

As shown in **Figure 12** and **Figure 13**, the effects of different proportions of oxacyclobutane monomer on curing rate and curing degree were tested. 2.5% Photoinitiator-3 triaryliodonium hexafluorophosphate (single salt) was used as cationic photoinitiator, 0.5% anthracene compound was used as sensitizer, and active diluent was 97%. The ratios of ternary epoxy and quaternary epoxy are 10:0, 8:2, 6:4, 4:6, 2:8, and 0:10, respectively. From **Figure 12** and **Figure 13**, with four-membered epoxy monomer content increasing, the light curing rate is also increasing, when four-membered epoxy monomers and three-membered to speak when the proportion of the curing rate of epoxy monomers fastest, continue to improve the four-membered monomer ratio of epoxy curing rate decreased, comprehensive consider choosing four-membered epoxy: three-membered epoxy = 8:2 as the best added.

2.1.5. Effect of Curing Temperature on Photocuring Rate

Studies have showed that photopolymerization is initiated after a certain amount of heat is given, which can also effectively reduce the induction period with the help of external energy input. Taking 2.5% Photoinitiator-3 triaryliodonium hexafluorophosphate (single salt) as cationic photoinitiator, 0.5% anthracene compounds as sensitizer, 97% as active diluent, and the ratio of quaternary epoxy to ternary epoxy is 8:2. Photo-DSC tests were conducted at temperatures of 20˚C, 40˚C, 60˚C, 80˚C and 100˚C, respectively. The testing results listed in **Figure 14** and **Figure 15**, show that the photocuring rate increases with the increase of curing temperature, and the fastest curing rate is achieved at 80˚C, while the photocuring rate decreases with the temperature increasing. Possibly due to the Photoinitiator-3 cationic photoinitiator will decompose and lose its photoactivity at about 100˚C. Wherefore, when the curing temperature is 80˚C, it has the fastest light curing rate and the highest heat release per unit mass, so 80˚C is selected as the best curing temperature.

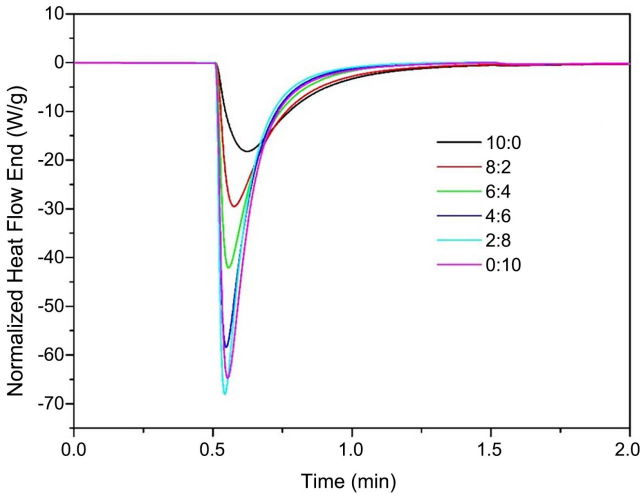

Figure 12. Influence of non-proportional ternary and quaternary epoxides on the photochemical rate.

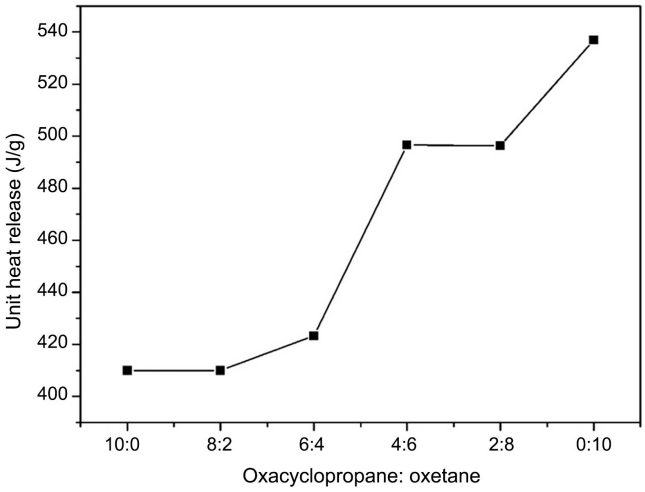

Figure 13. Influence of different proportions of quaternary epoxides on curing degree.

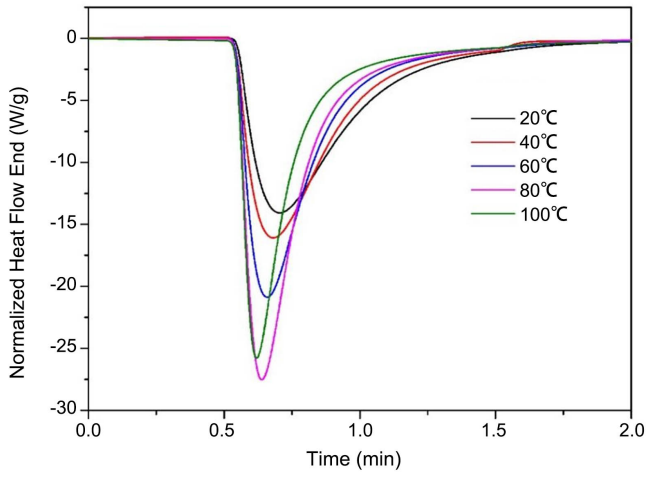

Figure 14. Effect of curing temperature versus photocuring rate.

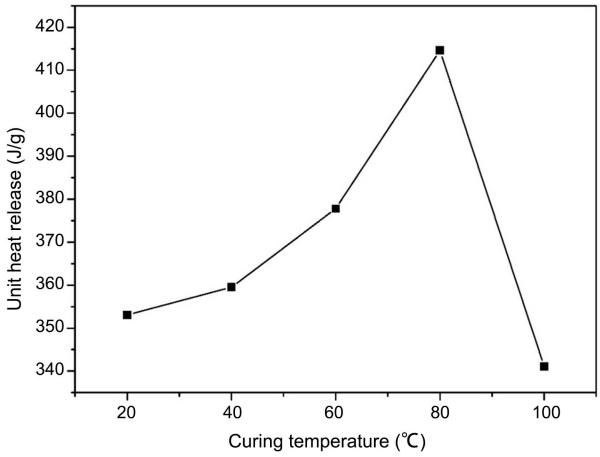

Figure 15. Influence of curing temperature versus curing degree.

2.1.6. Effect of Nano Silica Content on Photocuring Rate

Nano-SiO_2 has a strong UV absorption capacity, and it will compete with photoinitiators to absorb UV light. As shown in **Figure 16** and **Figure 17**, photoinitiators cannot generate enough free radicals or protic acid, resulting in low curing degree of the film and affecting the overall performance of the film, so the addition amount of nano-SiO_2 needs to be optimized. **Figure 16** and **Figure 17** have shown that the different nanometer SiO_2 content light curing rate and the influence of the curing degree. It can be seen from **Figure 16** and **Figure 17** that with the increasing amount of nano-SiO_2 added, the curing rate and curing degree of the system are constantly decreasing. When the amount of addition is less than 0.4%, the effect on the curing rate and degree of curing is small. Hence, the optimal addition amount of nano-SiO_2 should be less than or equal to 0.4%.

2.1.7. Effect of Nano-SiO_2 Content on Corrosion Resistance of Coating

As shown in **Table 2** and **Figure 18**, when the addition amount of nano-SiO_2 is none, the corrosion resistance of the coating is poor, and the corrosion area of the 72-h neutral salt spray experiment is greater than 10%. With the increase of the addition amounts of nano-SiO_2 (0.2% - 1.0%), the white rust area of the coating for 72 h neutral salt spray corrosion is stable in the range of 3% - 4%. Considering the influence of nano-SiO_2 on the curing rate and degree of the coating, 0.2% - 0.4% is selected as the optimal addition amount of nano-SiO_2.

2.2. Preparation of Passivation Film for UV-LED Curing Cationic System

2.2.1. Substrate Pretreatment

Take a piece of hot aluminum-zinc steel plate with the size of 75 mm × 150 mm × 1 mm. First, smooth the burres on the edge of the steel plate with sandpaper. Then, soak the steel plate in water solution with 2% degreasing agent at room temperature for 10 min before taking it out. Finally, the surface of the steel plate is wiped with acetone, process as shown in **Figure 19**.

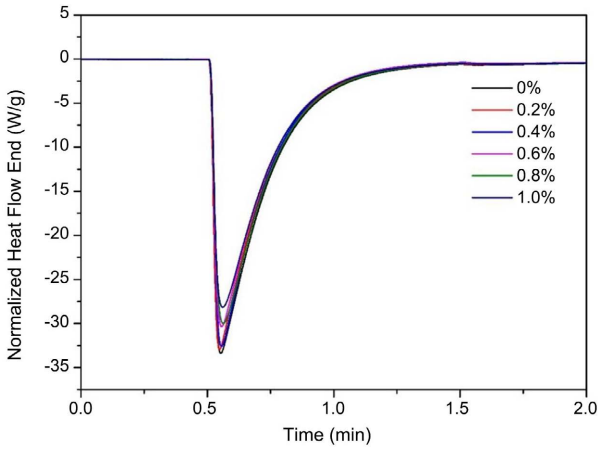

Figure 16. Influence of nano-SiO_2 addition amount on photocuring rate.

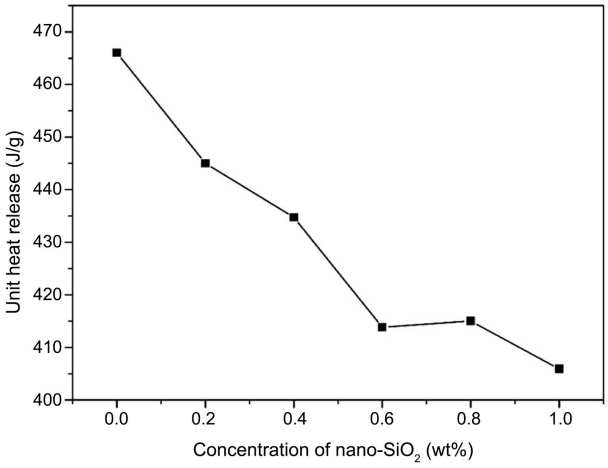

Figure 17. Influence of addition amount of nano-SiO_2 on curing degree.

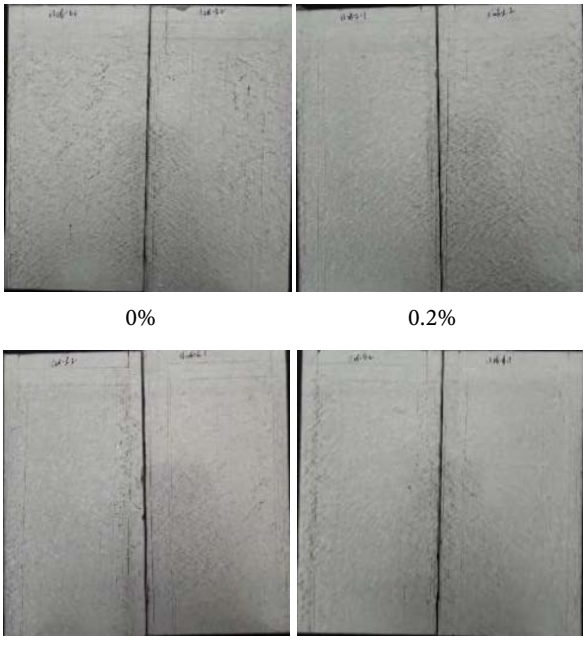

0.8% 1.0%

Figure 18. Neutral salt spray experiment of passivation films with different nano-SiO_2 contents in 72 h.

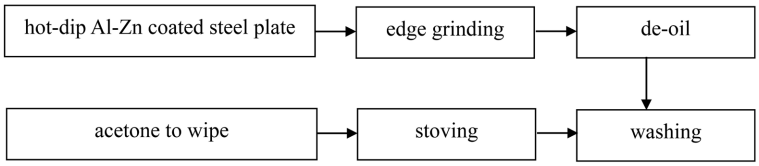

Figure 19. Pretreatment process flow of hot aluminum-zinc steel plate.

Table 2. Passivation film with different nano-SiO_2 contents of 72 h neutral salt spray experimental corrosion area data.

SiO_2 contents wt%	72 h neutral salt spray test corrosion area
0%	>10%
0.2%	3% - 4%
0.4%	3% - 4%
0.6%	3% - 4%
0.8%	3% - 4%
1.0%	3% - 4%

2.2.2. Preparation of Cationic Photocurable Passivating Film

Take a clean small beaker and add 2 - 3 g of epoxy oligomer into it, then add 5 - 6 g of active diluent mixed by 8:2 of quaternary epoxy and ternary epoxy, and then add 0.2 g of nano-SiO_2 dispersion (Shanghai Chemical Company, China). After that, 0.25 g of Photoinitiator-3 cationic photoinitiator and 0.05 g of anthracene sensitizer were added. Finally, 0.5 - 1.5 g of additive was added and stirred for 30 min to obtain the cationic photocurable passivation solution. Passivation solution is evenly coated on the surface of the steel plate with a 1.5 μm extruding coating rod. Thus, a cationic photocurable passivation film is obtained by putting it into a UV-LED exposure machine with an energy of 150 mJ/cm^2.

2.3. Testing and Analysis

2.3.1. Routine Performance Testing of Passivating Film

In order to meet the application requirements, there is a general requirement for the performance of passivation film in the industry, as shown in **Table 3**.

Table 3. Routine performance testing items and performance indexes of passivation film.

Indicator	Value
Membrane heavy	1.0 - 2.0 g/m^2
Adhesion (box 5 × 5)	0
High temperature yellowing resistance (200˚C × 20 min)	ΔE ≤ 3
Alkaline resistance (0.1%NaOH soaked at room temperature for 1 hr)	ΔE ≤ 3
Acid resistance (soak 0.1%HCl at room temperature for 1 hr)	ΔE ≤ 3
Medium alkali degreasing resistance (medium alkali degreasing agent FC-346 soaked at 60˚C for 2 min)	ΔE ≤ 3
The fingerprint resistance	ΔE ≤ 1
Boiling water resistance (100˚C boiling water immersion 2 h)	ΔE ≤ 3
Solvent resistance (80 percent alcohol wipe 20 times)	≥3

2.3.2. Resistance of Passivation Film to Neutral Salt Spray Corrosion (NSST)

The neutral salt spray testing was carried out according to GB 10125-2012 (Wuxi, China). The corrosion solution was 5% NaCl solution, the pH is 6.5 - 7.2, the experimental temperature was 35˚C ± 2˚C, the settlement was 1 - 2 mL per hour, the sample plate size was 75 mm × 150 mm, the surface was flat without oil stains, no damage, and the edge was without burns. The edges of the samples were sealed and protected with transparent tape. After continuous spraying for 72 h, the samples were evaluated according to the corrosion area of the samples. At present, the basic requirement of corrosion resistance of passivation film of commercial hot aluminum-zinc steel plate is that the neutral salt spray corrosion area of 72 h is less than 5%.

2.3.3. Resistance Test of Passivated Film to Electrochemical Corrosion

The electrochemical performance of the coating is mainly measured by AC impedance spectroscopy (EIS) and Tafel polarization curve, which is an effective method to evaluate the corrosion behavior of the material. The specific device and circuit connection are shown in **Figure 20**.

The electrochemistry workstation with three electrodes system was used for the testing (Shanghai, China). The photocurable hot aluminum-zinc steel plate was the working electrode, the saturated calomel electrode as the reference electrode, and the platinum plate electrode was the auxiliary electrode. NaCl solution with mass fraction of 3.5% was used as the corrosive medium, and the working area was 1 cm^2. The testing was carried out at room temperature. AC impedance spectrum testing frequency range was set as 0.01 - 100,000 Hz. Open circuit voltage (OCP) testing was carried out after the circuit connection was completed, and AC impedance spectrum (EIS) testing was carried out after the open circuit voltage (OCP) was stabilized. The experimental data was fitted with Z-View software.

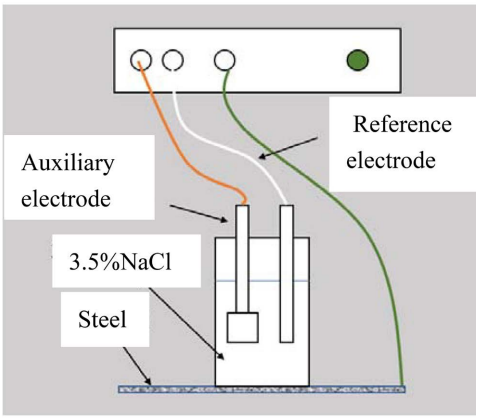

Figure 20. Schematic diagram of electrochemical testing device.

The scanning range of Tafel polarization curve testing was from −1.7 V to −0.5 V, and the scanning rate was 20 mV/s. The testing was carried out at room temperature. Open circuit voltage (OCP) testing was carried out after the circuit connection was completed, and Tafel polarization curve test was carried out after the open circuit voltage (OCP) was stabilized. The experimental data were processed by the software attached to the electrochemical workstation.

2.3.4. Measurement of Passivated Film by Fourier Transform Infrared Spectroscopy

Fourier transform infrared spectroscopy (FT-IR) is an important characterization method in the field of organic chemistry. Different functional groups have different absorption peaks in different wavelength ranges. The degree of curing of coatings was characterized by the comparison of the changes of absorption peaks of characteristic functional groups before and after curing. The infrared spectrometer used in this experiment is the IR Tracer-100 infrared spectrometer of Shimadzu Company, Kyoto, Japan, and the scanning range is 4000 cm^{-1} - 400 cm^{-1}.

2.3.5. Analysis of Surface Morphology of Passivation Film

Scanning electron microscopy (SEM) can directly image the surface of materials as an effective method to observe the microstructure of materials. Hitachi Flex-SEM 1000II (Japan, Tokyo) type scanning electron microscope was used to observe the microstructure of the coating surface, the main magnification was 1000 and 3000 times, respectively, the testing acceleration voltage was 20 kV.

3. Results and Discussion

3.1. Routine Performance Testing of Passivating Film

Table 4 lists the conventional performance testing results of cationic photocurable passivation film. It can be seen from Table 4 that the conventional performance of cationic photocurable passivation film is good, and all of them meet the requirements of downstream users of hot aluminum-zinc steel plate.

Table 4. Conventional performance testing results of cationic photocurable passivation film.

Indicator	Value	Test Results
Membrane heavy	1.0 - 2.0 g/m^2	1.0 - 2.0 g/m^2
Adhesion (box 5 × 5)	0	0
High temperature yellowing resistance (200˚C × 20 min)	ΔE ≤ 3	0.42
Alkaline resistance (0.1%NaOH soaked at room temperature for 1hr)	ΔE ≤ 3	2.26
Acid resistance (soak 0.1%HCl at room temperature for 1 hr)	ΔE ≤ 3	0.66
Medium alkali degreasing resistance (medium alkali degreasing agent FC-346 soaked at 60˚C for 2 min)	ΔE ≤ 3	0.24
The fingerprint resistance	ΔE ≤ 1	0.09
Boiling water resistance (100˚C boiling water immersion 2 h)	ΔE ≤ 3	1.84
Solvent resistance (80 percent alcohol wipe 20 times)	≥3	3

3.2. Resistance of Passivation Film to Neutral Salt Spray Corrosion (NSST)

As shown in Figure 21, two pieces of steel plate surface passivation film of 72 h neutral salt spray corrosion performance were tested. By Table 5 to know corrosion of steel plate surface area of 3% - 4% when to 72 h salt spray corrosion time. It less than aluminum-zinc steel plate, steel belt and Baosteel pipe coating neutral salt spray resistance of small code requirements of 5%, and shown that passivation membrane has a relatively good corrosion resistant performance.

3.3. Resistance Test of Passivated Film to Electrochemical Corrosion

3.3.1. Tafel Polarization Curve and AC Impedance Spectroscopy (EIS) Test

Electrochemical tests were carried out on different surface treatments (fingerprint resistance, chromate passivation, cationic photocurable coating) and untreated hot coated aluminum-zinc steel plates to compare with the corrosion resistance of four different steel plates. The Tafel polarization curve and AC impedance spectrum (EIS) were measured at room temperature using 3.5% neutral NaCl solution as corrosive medium.

1) Tafel polarization curve testing

Figure 22 shows that the comparison of hot-dip aluminum-zinc steel plate, chromate passivation film, fingerprint resistant film and cationic UV-curable coatings from the corrosion potential was increased, and the anode polarization curve and the polarization current of cathodic polarization curve is relatively lower than that of hot-dip aluminum-zinc steel plate, an indicative of the process of cationic UV-curable coatings for corrosion inhibition effect of cathode and

anode reactions. The data onto Table 6, electrochemical workstation with the software were obtained from the calculation on the basis of by the table to know, since the cationic UV-curable coatings corrosion current with hot-dip aluminum-zinc steel plate is two orders of magnitude, slightly below the chromate passivation film and commercial fingerprint resistant passivation film, it shows that cationic UV-curable coating corrosion resistance is relatively lower than the chromate passivation film and fingerprint resistant coating but the overall difference.

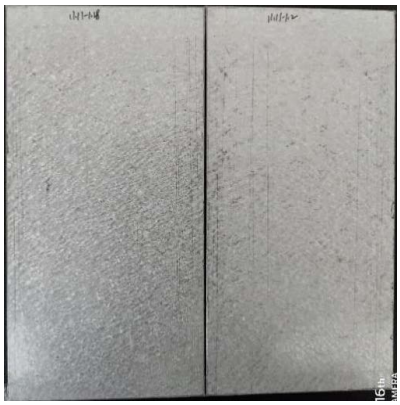

Figure 21. Resistance testing of passivation film to 72 h neutral salt spray corrosion.

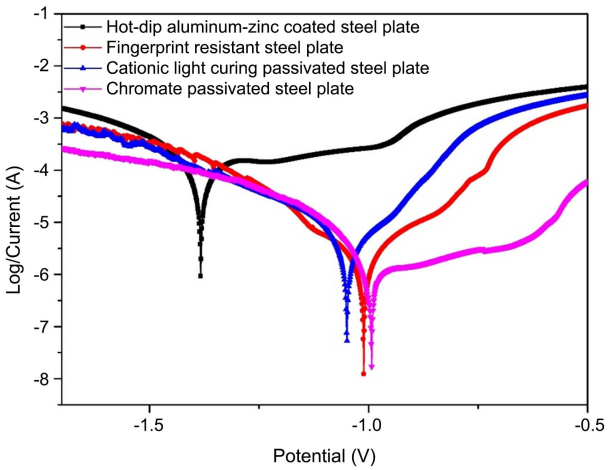

Figure 22. Tafel polarization curves of the four samples.

Table 5. Testing data of resistance testing of passivation film to 72 h neutral salt spray corrosion.

sample no.	1 - 15	1 - 16
conditions	3.5% neutral NaCl solution was sprayed continuously for 72 h	
curing grade	5	5
film thickness	1.18	1.16
results	Corrosion area for 72 h is 3% - 4%	

Table 6. Tafel polarization curve data of the four samples.

Sample	Corrosion potential /V	self-corrosion current/A·cm^{-2}
Hot aluminum plated zinc sheet	−1.383	1.833×10^{-4}
Chromate passivating plate	−0.993	2.544×10^{-6}
Fingerprint resistant plate on the market	−1.012	3.057×10^{-6}
Cationic light curing coating plate	−1.049	4.712×10^{-6}

2) AC impedance spectroscopy (EIS) testing

Figure 23 shows the alternating current impedance spectra (Nyquist) of four samples. It can be seen that the impedance of cationic photocurable coating, chromate passivation film and fingerprint resistant film is greatly improved compared with that of hot aluminum-zinc steel plate without surface treatment, and the impedance value of cationic photocurable coating is about 35 times that of hot aluminum-zinc steel plate, but lower than that of chromate passivation film and fingerprint resistant film on the market, an indicative of the diffusion of the corrosive medium in the cationic photocurable coating being more difficult and the coating has better corrosion resistance. At the same time, the corrosion resistance of the coating is slightly lower than that of chromate passivation film and fingerprint resistant film, which is consistent with the results in **Figure 22** and **Table 6**.

3.3.2. Brine Immersion Test

Using 3.5% neutral NaCl solution as a corrosive medium, the cationic photocurable coating plate was soaked in brine. Before soaking, the steel plate was edge sealed with 3M tape. The soaking temperature was room temperature, and the soaking time was 0 h, 6 h, 12 h, 24 h, 48 h and 72 h, respectively. The obtained results were fitted with Z-View software, and the fitted data were plotted by Origin software.

The experimental results show that the cationic photocurable coating exhibits the excellent barrier properties at the initial soaking stage (0 h, 6 h), and its equivalent circuit is shown in **Figure 24(a)**. The corrosive medium slowly penetrates into the surface of the metal substrate, thus causing corrosion on the surface of the metal substrate with an extension of immersion time (12 h, 24 h, 48 h). At this time, the corrosion products will enter the pores of the coating, thus inhibiting the diffusion of the corrosive medium in the coating. The equivalent circuit of this process is shown in **Figure 24(b)**. In the late soaking period (72 h), the coating has basically lost its shielding function, and the corrosive medium can easily diffuse from the coating surface into the surface of the metal matrix. Its equivalent circuit is shown in **Figure 24(c)**.

Generally, the resistance of the coating to corrosive media can be indicated by the magnitude of the alternating impedance modulus of the coating in the low frequency region (0.01 Hz), that is, the corrosion resistance of the coating is bet-

ter with the larger alternating impedance modulus of the coating at low frequency. It can be seen from Figure 25 and Figure 26 that the barrier of the cationic photocurable coating decreases gradually with the extension of immersion time in 3.5% NaCl solution, which indicates that the corrosive medium penetrates from the coating surface to the surface of the metal substrate and causing corrosion of the metal substrate with the extension of immersion time. According to the alternating current impedance spectra (Nyquist), it can be found that the low-frequency alternating impedance modulus of the coating decreased slightly at the beginning of soaking (0 h, 6 h), but the change was small, and its frequency/phase diagram basically did not change. This indicates that the coating has a good barrier to the corrosive medium in this time. In the middle soaking period (12 h, 24 h, 48 h), the low frequency AC impedance modulus of the coating decreased significantly compared with the initial soaking period. However, the low frequency AC impedance modulus of the coating decreased to a small extent during 12 - 48 h. At this stage, the corrosive medium has diffused from the coating surface to the surface of the metal matrix. At this time, the corrosion

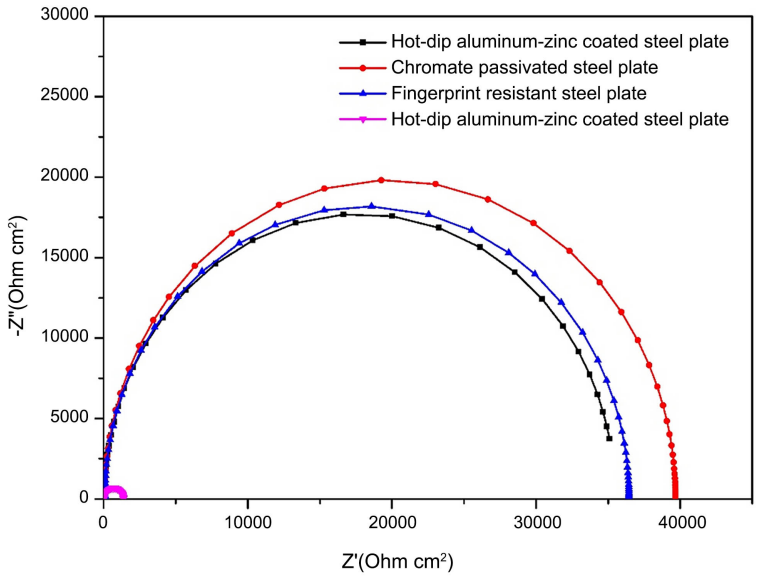

Figure 23. Nyqusit plots of AC impedance for four types of templates.

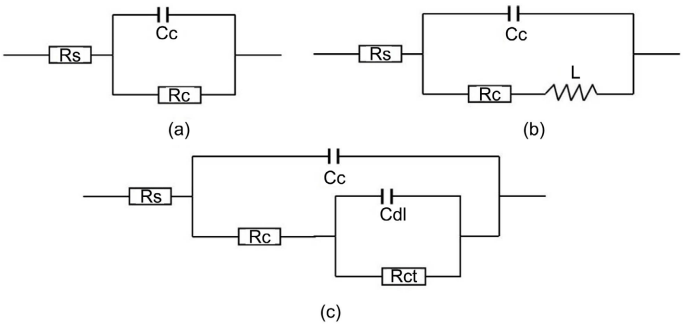

Figure 24. Equivalent circuit model of cationic photocurable coating in different time stages of immersion experiment.

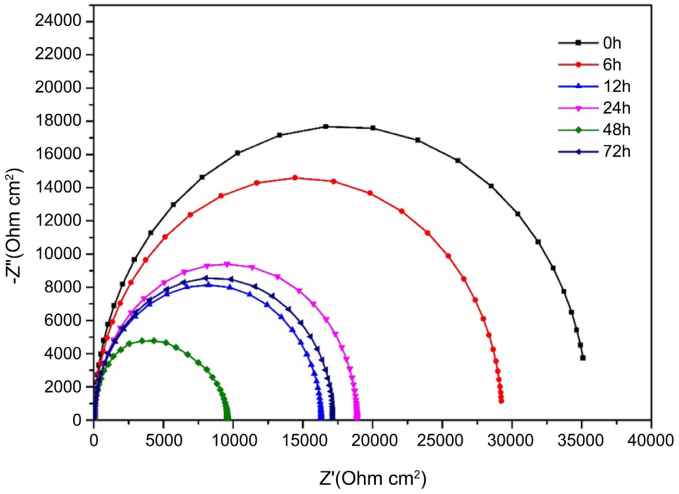

Figure 25. Nyquist diagram of AC impedance of cationic photocurable coating in brine immersion.

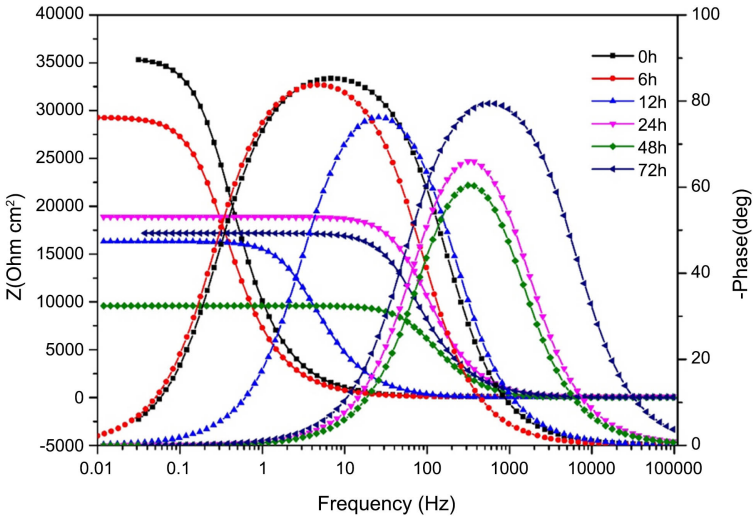

Figure 26. Bode diagram of ac impedance of cationic photocurable coating soaked in brine.

products will fill the pores of the coating, thus inhibiting the continuous corrosion. It can also be seen from Nyquist diagram that the arc radius of the coating does not change much after soaking for 12 h, 24 h and 48 h, indicating that the coating still has good protective performance after soaking for 48 h. At the latest soaking stage (72 h), the low-frequency AC impedance modulus of the coating decreased sharply, indicating that the structure of the coating had been seriously damaged at this stage, but the low-frequency AC impedance modulus of the coating was still higher than that of the hot aluminum-zinc steel plate.

3.4. Measurement of Passivated Film by Fourier Transformation Infrared Spectroscopy

Figure 27(a) shows the infrared spectrum of the cationic photocurable passivation solution before curing, in which 979 cm^{-1} and 788 cm^{-1} are the C-O-C ab-

sorption peaks of oxacyclobutane and the characteristic peaks of the quaternary epoxy structure. The characteristic absorption peak of C-O-C of ethylene oxide is at 910 cm^{-1}. Figure 27(b) shows the infrared spectrum of the cationic photocurable passivation solution after curing. Compared with Figure 27, it can be obviously found that the characteristic peaks of quaternary epoxide in oxacyclobutane structure at 979 cm^{-1} and 788 cm^{-1} are significantly smaller, the absorption peak at 979 cm^{-1} is almost disappeared, and the characteristic peaks of ethylene oxide at 910 cm^{-1} are also significantly smaller.

3.5. Analysis of Surface Morphology of Passivation Film

Scanning electron microscope (SEM) testing results are shown in Figure 28, and shows that the passivation solution is coated on the silicon wafer with the same coating method for testing. A is 1000 times of film amplification, B is 3000 times

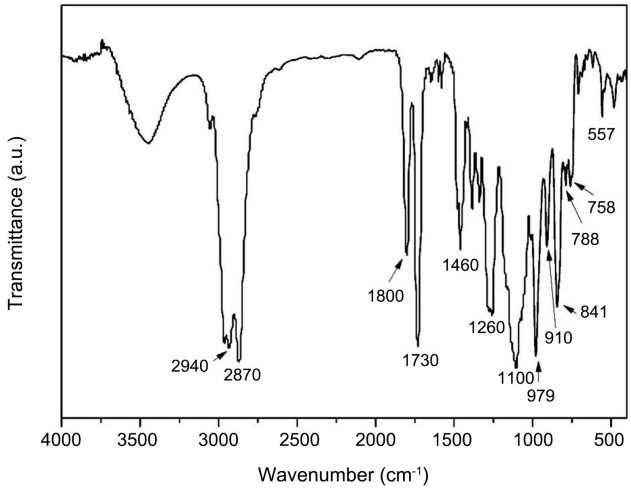

(a)

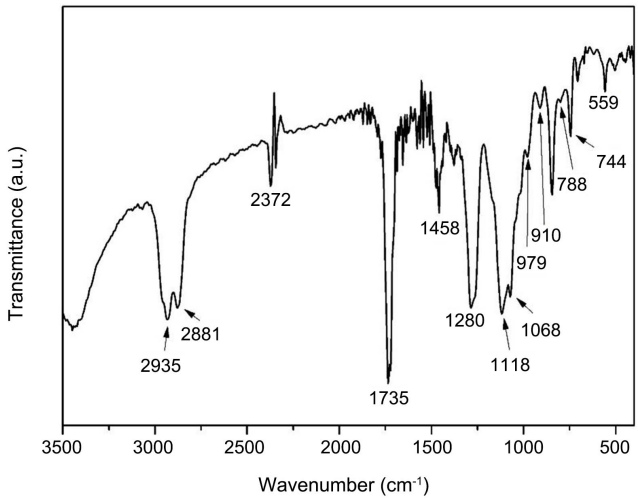

(a)

Figure 27. Infrared spectrum test results of passivation solution (a) before curing, (b) after curing.

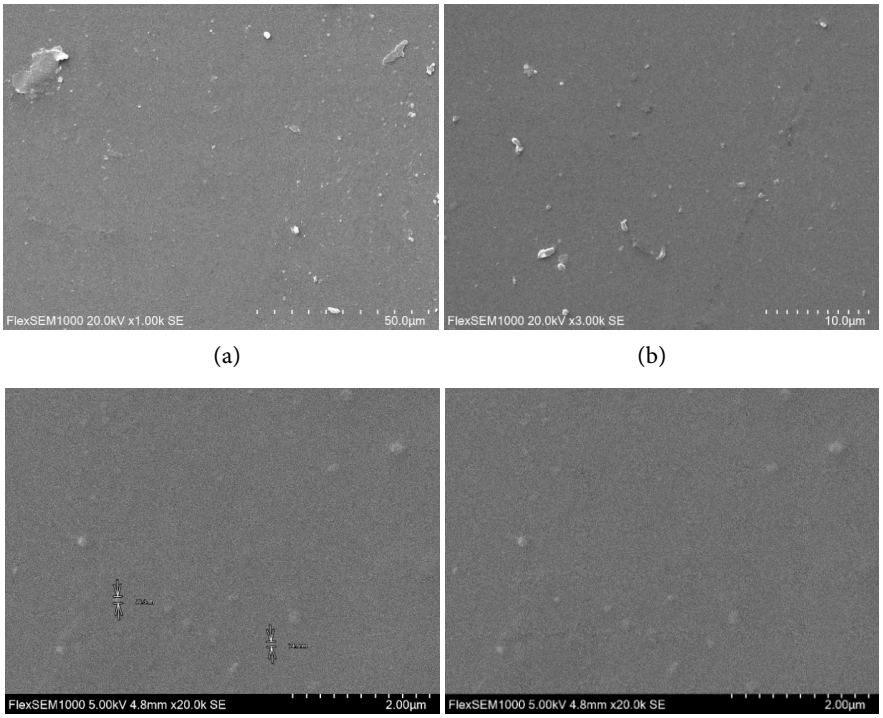

Figure 28. SEM images of the cationic photocurable passivation films.

of film amplification, and C and D are 20,000 times of nano SiO_2 dispersion. Hitachi FlexSEM1000 scanning electron microscope is used for observation at 1000- and 3000-times magnification. **Figure 28(a)** and **Figure 28(b)** are SEM photos at 1000- and 3000-times magnification, respectively. As can be seen from the **Figure 28**, the surface of the passivation film is compact and uniform, with no obvious cracks. As can be seen from **Figure 28**, the SEM picture of the modified nano-SiO_2 dispersion at 20,000 times of 28c and 28d is shown in **Figure 28**. The particle size of nano-SiO_2 is basically below 100 nm and the distribution is relatively uniform, without agglomeration. It is also proved from the side that the cationic light curing shrinkage is relatively lower.

4. Conclusion

The cationic photocurable passivation solution obtained is a solvent-free formula. Compared with the commercially available fingerprint passivation liquid, the performance of the passivation film is slightly lower than that of the fingerprint passivation film, but the difference is quite small. The cost is about 10 times that of the commercially available fingerprint resistant passivation solution but considering the solid content of the commercially available fingerprint resistant passivation solution is only 20% - 30%, the use cost of the cationic light curing passivation solution is higher than the traditional passivation solution at present. As a new green coating technology, photocuring technology is in line with the national energy conservation and emission reduction policy, with high intensity of equipment and simple coating process. In the future, the photocuring technolo-

gy is likely to replace traditional passivation technology. The main conclusions are drawn as follows: 1) The photoinitiation rate of four different photoinitiators and sensitizers was measured by photo-DSC. The photoinitiation system of triaryl sulfonium liufluorophosphate and an anthracene sensitizer was studied. The results showed that the ratio of active diluent TCM 104 to UVR 6110 was 8:2, and the pre-baking temperature was 80˚C. Under the condition of adding 0.2% nano-SiO_2, the system has the fastest photocuring rate. On this basis, the cationic photocurable passivation solution was prepared by adding 20% - 40% epoxy resin and a small number of various additives. 2) Through a series of testing to study the properties of cationic light curing passivation film, the results showed that the cationic passivation film has excellent adhesion (0 level), high temperature yellow (ΔE = 0.42), acid resistance (Na E = 0.66), alkali resistance (Na E = 2.26), alkali defatting resistance (Si E = 0.24), solvent resistance (3 level), fingerprint resistance (ΔE = 0.09) and boiling water resistance (Nd E = 1.84), electrochemical and 72-h neutral salt spray test (white rust area of 3% - 4%) results showed that the passivated film has relatively good corrosion resistance. The passivated film SEM testing shows that the surface of the film is relatively flat and almost no pores and cracks.

Acknowledgements

This work was supported by the National Basic Research Program of China (863 Program, 2009AA03Z529). We are grateful to Dr. Jing Yuan for her proof-reading of this manuscript.

Conflicts of Interest

The authors declare no conflicts of interest regarding the publication of this paper.

References

[1] Ghazali, S.K., Adrus, N., Majid, R.A., Ali, F. and Jamaluddin, J. (2021) UV-LED as a New Emerging Tool for Curable Polyurethane Acrylate Hydrophobic Coating. *Polymers*, **13**, 487-498. https://doi.org/10.3390/polym13040487

[2] Belfield, K.D. and Crivello, J.V. (2003) Photoinitidted Polymerization. Oxford University Press, Washington DC, 285-295. https://doi.org/10.1021/bk-2003-0847

[3] Crivello, J.V. and Bulut, U. (2005) Photoactivated Cationic Ring-Opening Frontal Polymerizations of Oxetanes. *Designed Monomers and Polymers*, **8**, 517-531. https://doi.org/10.1163/156855505774597803

[4] Crivello, J.V. and Sasaki, H. (1993) Structure and Reactivity Relationships in the Photoinitiated Cationic Polymerization of Oxetane Monomers. *Journal of Macromolecular Science*, *Part A*: *Pure and Applied Chemistry*, **30**, 189-206. https://doi.org/10.1080/10601329308009399

[5] Crivello, J.V. (2015) "Kick-Starting" Oxetane Photopolymerizations. *Journal of Polymer Science Part A Polymer Chemistry*, **52**, 2934-2946. https://doi.org/10.1002/pola.27329

[6] Crivello, J.V. (2015) Investigations of the Reactivity of "Kick-Started" Oxetanes in

Photoinitiated Cationic Polymerization. *Journal of Polymer Science Part A*: *Polymer Chemistry*, **53**, 586-593. https://doi.org/10.1002/pola.27479

[7] Xu, J.C., Jiang, Y., Zhang, T., Dai, Y.T., Yang, D.Y., Qiu, F.X., Yu, Z.P. and Yang, P.F. (2018) Synthesis of UV-Curing Waterborne Polyurethane-Acrylate Coating and Its Photopolymerization Kinetics Using FT-IR and Photo-DSC Methods. *Progress in Organic Coatings*, **122**, 10-18. https://doi.org/10.1016/j.porgcoat.2018.05.008

[8] Gao, J., Zhang, Y. and Zhang, C. (2010) Nonisothermal Co-Polymerizing Behavior and Thermal Properties of Methylacyloxylpropyl-POSS with Styrene. *Polymer-Plastics Technology and Engineering*, **49**, 531-540. https://doi.org/10.1080/03602550903532216

[9] Decker, C. (1998) The Use of UV Irradiation in Polymerization. *Polymer International*, **45**, 133-141. https://doi.org/10.1002/(SICI)1097-0126(199802)45:2%3C133::AID-PI969%3E3.0.CO;2-F

[10] Tiwari, A. and Polykapov, A. (2015) Photocured Materials. Royal Society of Chemistry, Cambridge, 1-9. https://doi.org/10.1039/9781782620075-00001

[11] Aguirresarobe, R.H., Irusta, L. and Fernández-Berridi, M.J. (2014) UV-Light Responsive Waterborne Polyurethane Based on Coumarin: Synthesis and Kinetics of Reversible Chain Extension. *Journal of Polymer Research*, **21**, 1-9. https://doi.org/10.1007/s10965-014-0505-5

[12] Kissinger, H.E. (1957) Reaction Kinetics in Differential Thermal Analysis. *Analytical Chemistry*, **29**, 1702-1706. https://doi.org/10.1021/ac60131a045

[13] Atarsia, A. and Boukhili, R. (2010) Relationship between Isothermal and Dynamic Cure of Thermosets via the Isoconversion Representation. *Polymer Engineering and Science*, **40**, 607-620. https://doi.org/10.1002/pen.11191

[14] Crane, L.W., Dynes, P.J. and Kaelble, D.H. (1973) Analysis of Curing Kinetics in Polymer Composites. *Journal of Polymer Science Part C Polymer Letters*, **11**, 533-540. https://doi.org/10.1002/pol.1973.130110808